Maximizing power production in a stack of microbial fuel cells using multiunit optimization method

Woodward, Lyne; Perrier, Michel; Srinivasan, Bala; Tartakovsky, Boris

Publisher's version / Version de l'éditeur:
http://dx.doi.org/10.1002/btpr.115
Biotechnology Progress, 25, 3, pp. 676-682, 2009-06-03

Maximizing Power Production in a Stack of Microbial Fuel Cells Using Multiunit Optimization Method

Lyne Woodward, Michel Perrier, and Bala Srinivasan
Dépt. de Génie Chimique, École Polytechnique de Montréal, Centre-Ville, Montréal, QC, Canada H3C 3A7

Boris Tartakovsky
Dépt. de Génie Chimique, École Polytechnique de Montréal, Centre-Ville, Montréal, QC, Canada H3C 3A7
Biotechnology Research Institute, National Research Council of Canada, 6100 Royalmount Ave., Montréal, QC, Canada H2P 2R2

DOI 10.1021/bp.115
Published online June 3, 2009 in Wiley InterScience (www.interscience.wiley.com).

This study demonstrates real-time maximization of power production in a stack of two continuous flow microbial fuel cells (MFCs). To maximize power output, external resistances of two air–cathode membraneless MFCs were controlled by a multiunit optimization algorithm. Multiunit optimization is a recently proposed method that uses multiple similar units to optimize process performance. The experiment demonstrated fast convergence toward optimal external resistance and algorithm stability during external perturbations (e.g., temperature variations). Rate of the algorithm convergence was much faster than in traditional maximum power point tracking algorithms (MPPT), which are based on temporal perturbations. A power output of 81–84 mW/L_A (A = anode volume) was achieved in each MFC.
 Biotechnol. Prog., 25: 676–682, 2009
Keywords: microbial fuel cell, multiunit optimization, stack

Introduction

Power generation in a microbial fuel cell (MFC) from renewable carbon sources is a potential alternative to fossil fuel utilization.[1,2] In a MFC, anodophilic microorganisms degrade organic matter and transfer electrons to the anode via nanowires or self-produced mediators.[3–5] Since the late 90s, when intensive MFC development began, power density in MFCs increased by several orders of magnitude.[6] Yet, attainable power density of a single MFC is relatively low, in a range of 50–200 W/m^3_A (A = anode chamber volume) and the working voltage is limited to 0.3–0.5 V.[7] Consequently, a stack of MFCs might be required to obtain the desired power output.[7,8] As in any other battery, power generation in a MFC strongly depends on the external resistance (load) so that maximum power is produced when the external load is equal to the internal resistance of the cell.[9] As MFC is a biological system, the internal resistance depends on environmental factors such as temperature and influent composition. As a consequence, timely adjustment of the external load is required to maximize power production.

The classical approach of real-time optimization consists of two steps.[10,11] First, a model of the process is used to numerically calculate the optimum. Next, the model is updated using the available measurements and the updated model is then used for numerical optimization. However, building and maintaining a sufficiently detailed model of a MFC represents a challenge in itself. Also, the solution does not converge to the optimum if the model structure does not adequately describe the process.[12]

Extremum-seeking is an alternative approach[13,14] where optimization is achieved by following the necessary conditions of optimality, i.e., in an unconstrained case, forcing the gradient to zero. For gradient estimation, perturbation methods[15] can be used, when measurements of the performance criterion are available. If only auxiliary measurements are available, a model-based gradient estimation approach is needed.[16] Maximum power point tracking (MPPT) algorithms used in photovoltaic systems are also based on an estimation of the gradient. These algorithms can also be used to maximize the electrical power of microbial fuel cells in real-time. The perturbation and observation method is the most popular due to its simplicity of implementation.[17]

The multiunit optimization method[18,19] is a recent technique for gradient estimation. Here, multiple identical units are driven with inputs that are offset by a design parameter. The gradient is obtained by a finite difference of the unit outputs, which is then forced to zero. This method has shown faster convergence than the perturbation method mainly because perturbations are in the "units" dimension instead of time dimension. The dynamics of the units are compensated by taking the difference between two units. Thus, there is no need to wait for the dynamics to die down, thereby reducing the time required for optimization. However, the fact that the units have to be identical is a very

Correspondence concerning this article should be addressed to B. Srinivasan at bala.srinivasan@polymtl.ca.

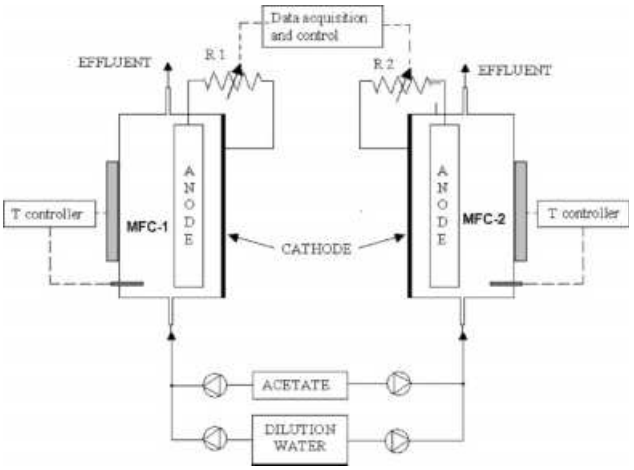

Figure 1. Experimental setup.

strong assumption which does not depict a realistic scenario. The method can be modified to make it applicable to processes with similar but nonidentical units by introducing correctors. In this article, the multiunit optimization method is used for real-time power output maximization of a stack of two MFCs.

Materials and Methods

MFC design, instrumentation, and operation

Experiments were carried out in two continuous flow air–cathode membraneless MFCs.[20] Each MFC was constructed with a series of polycarbonate plates. The anodic chamber volume of each cell was 100 mL. The cells were equipped with lines for influent, effluent, liquid recirculation, and gas exits, as shown in Figure 1. The anode was made of a 5 mm thick graphite felt measuring 10 × 5 cm^2 (GFA5, Speer Canada, Kitchener, ON, Canada). The cathode was made of a 10 × 5 cm^2 gas diffusion electrode with a Pt load of 0.5 mg/cm^2 (GDE LT 120EW, E-TEK Division, PEMEAS Fuel Cell Technologies, Somerset, NJ). The distance between the anode and cathode was 1.5 cm.

The MFCs were inoculated with 5 mL of homogenized anaerobic sludge (Lassonde Industries, Rougemont, QC, Canada). A stock solution of carbon source was fed using an infusion pump (model PHD 2000, Harvard Apparatus, Canada) at a rate of 2.5–5 mL/d, which corresponded to an influent acetate concentration of 700–1,400 mg/L. One milliliter of trace metals stock solution was added to 1 L of the dilution water. The dilution water was fed at a rate of 146 mL/d using a peristaltic pump (Cole-Parmer, Chicago, IL) providing a retention time of 10 h. Another peristaltic pump was used for liquid recirculation at a rate of 0.57 L/h in external recirculation loop. MFC temperature was maintained at a preset value using a 5 × 10 cm^2 heating plate located on the anodic chamber side of the MFC, a thermocouple placed in the anodic chamber, and a temperature controller (Model JCR-33A, Shinko Technos Co., Osaka, Japan). For each MFC, four digitally controlled potentiometers connected in parallel were used to enable resistor variation from 12 to 252 Ω (Model X9C102 from Intersil, Milpitas, CA). Voltage was measured on-line using a data acquisition device (Labjack U12, Labjack Corp, Lakewood, CO).

Media composition and analytical measurements

The stock solution of carbon source was composed of (in g/L) acetate (40.0), yeast extract (6.7), NH_4Cl (18.7), KCl (148.1), K_2HPO_4 (64.0), and KH_2PO_4 (40.7). The stock solution of trace metals was prepared according to Ref.[21] and contained (in mg/L) $FeCl_2 \cdot 4H_2O$ (2000), H_3BO_3 (50), $ZnCl_2$ (50), $CuCl_2$ (30), $MnCl_2 \cdot 4H_2O$ (500), $(NH_4)_6MO_7O_{24} \cdot 4H_2O$ (50), $AlCl_3$ (50), $CoCl_2 \cdot 6H_2O$ (50), $NiCl_2$ (50), EDTA (500), and HCl (1mL). All solutions were filter sterilized and maintained at 4°C until use. Distilled water was used for solution preparation, and the chemicals and reagents used were of analytical grade. Acetate concentration was determined using a gas chromatograph (Sigma 2000, Perkin-Elmer, Norwalk, CT) equipped with a 91 cm × 4 mm i.d. glass column packed with 60/80 Carbopack C/0.3% Carbopack 20 NH_3PO_4 (Supelco, Mississauga, Ontario, Canada). More details on analytical methods are provided in Ref. 22.

Theory

Problem formulation

Consider a dynamic system with state $x \in R^n$ and input $u \in R^m$ that has to be operated so as to maximize a convex function $J(x,u)$ at steady state. The problem is shown below:

$$\max_u J(x,u) \tag{1}$$

$$\text{Subject to } \dot{x} = F(x,u) \equiv 0 \tag{2}$$

where $F(x, u)$ is the function describing the dynamics of the system, which is assumed to be stable. The necessary conditions of optimality[23] are given by:

$$\frac{dJ}{du} = \frac{\partial J}{\partial u} - \frac{\partial J}{\partial x}\left(\frac{\partial F}{\partial x}\right)^{-1}\frac{\partial F}{\partial u} = 0 \tag{3}$$

As in the steepest descent method for numerical optimization,[23] extremum seeking makes the process evolve in the direction of the gradient. However, instead of using the iteration index as in numerical methods of optimization, the iterations evolve in real time. The extremum-seeking control law is an integral controller that forces the gradient to zero:

$$\dot{\boldsymbol{u}} = \boldsymbol{k}\left(\frac{\boldsymbol{dJ}}{\boldsymbol{du}}\right) \tag{4}$$

where k is the controller gain. The key problem is the estimation of the gradient, which could be addressed using several methods.[24,25] The multiunit method provides an estimate of the gradient by finite differences as will be shown next.

The multiunit scheme

Multiunit optimization[18] requires a process with $(m + 1)$ identical units. The units are operated with input values that differ by an offset. For the application presented in this article, u is a scalar, i.e., $m = 1$. Then, $(m + 1) = 2$ identical units are required. The scheme is presented in Figure 2. The first unit is operated at the input value $\boldsymbol{u}_1 = \boldsymbol{u} - \frac{\Delta}{2}$ whereas the second unit is operated with input $\boldsymbol{u}_2 = \boldsymbol{u} + \frac{\Delta}{2}$. Then, the gradient estimated by finite difference between the two units is given by:

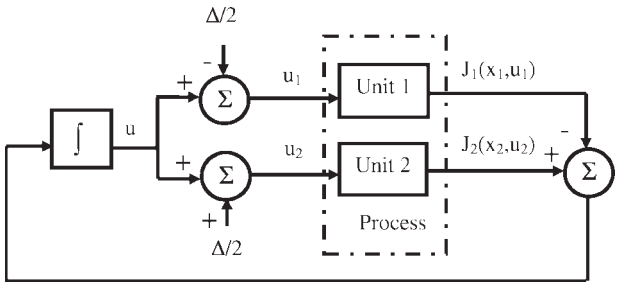

Figure 2. Schematic for multiunit optimization.

$$\hat{\boldsymbol{g}}(\boldsymbol{u}) = \frac{\boldsymbol{J}_2(\boldsymbol{x}_2, \boldsymbol{u}_2) - \boldsymbol{J}_1(\boldsymbol{x}_1, \boldsymbol{u}_1)}{\Delta} \tag{5}$$

and the extremum-seeking control law is given by:

$$\dot{\boldsymbol{u}} = \boldsymbol{k}\hat{\boldsymbol{g}}^{\boldsymbol{T}}(\boldsymbol{u}) \tag{6}$$

Both units follow the same control law and always keep an input offset of Δ from each other. The convergence of this scheme to a domain around the optimum has been proven despite the errors caused by the dynamics (which is assumed to be stable) and the error due to finite differences.[18] The multiunit scheme will force the units to converge to a domain around the optimum considering u^* is the averaged optimum of the two units. One unit converges to $u^* - \Delta/2$ and the other will converge to $u^* + \Delta/2$.

The main advantage of this approach is that the perturbation is along the dimension of the units, as opposed to the traditional methods where the perturbation is temporal. If temporal perturbations are used, it is important to wait until the system reaches steady state before the finite difference gradient can be evaluated. However, with the multiunit scheme, the dynamics of the two units could be assumed identical and would not interfere with the optimization. Thus, more rapid convergence could be achieved with multiunit optimization as opposed to other perturbation methods.

Multiunit optimization with nonidentical units

The main limitation of the multiunit scheme as presented in the previous section is the requirement of the two units being identical. In reality, the units used are not necessarily identical, and this difference between the units could cause the system to converge toward a false optimum which may not reflect the real optimum and/or could influence the stability of the scheme.

The differences between the various units can manifest in the following ways: differences in dynamics, differences in static responses, or differences in disturbance effects. The case considered in this article assumes the following: (i) the system has only one input, (ii) the dynamics are very fast compared to the optimization time-scale, i.e., the process can be considered quasi-static, (iii) no noise effects are considered, and (iv) the functions are convex.

Under these conditions, let the static characteristics of the two units be represented by $J_1(u_1)$ and $J_2(u_2)$. The relationship between the two static maps can be rewritten as:

$$\boldsymbol{J}_2(\boldsymbol{u}) = \boldsymbol{J}_1(\boldsymbol{u} + \beta) + \gamma + \overline{\boldsymbol{J}}(\boldsymbol{u}) \tag{7}$$

where $\beta = u_1^{\text{opt}} - u_2^{\text{opt}}$ and $\gamma = J_2(u_2^{\text{opt}}) - J_1(u_1^{\text{opt}})$, u_1^{opt} and u_2^{opt} are the optima of the first and second unit, respectively. The transformation is to bring the second unit to the same coordinates as those of the first unit by shifting the input and the output of the second unit. In the neighborhood of the optimum, if the difference in curvature between the two units at their respective optima is negligible, it can be assumed that $\overline{\boldsymbol{J}} \cong 0$. An example of such different static characteristics for two units is presented on Figure 3.

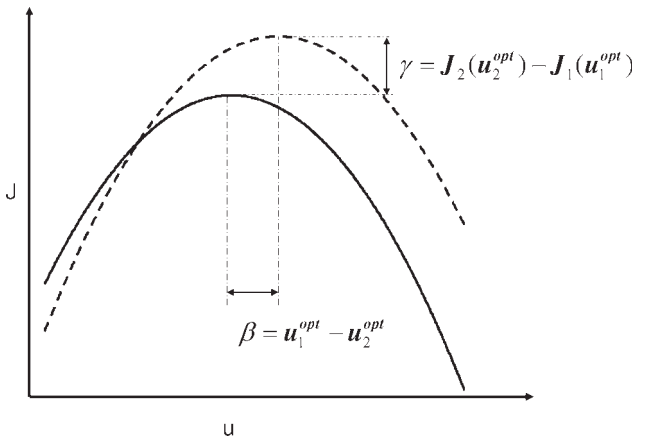

Figure 3. Example of differences in static characteristics of two units.

Differences in units cause the scheme to converge to a value away from the desired optimum. As given in Ref. 26, the converged solution is given by (see Appendix A)

$$u^* \cong \frac{u_1^{\text{opt}} - u_2^{\text{opt}}}{2} - \frac{\gamma}{(\Delta + \beta)\frac{\partial^2 J_1}{\partial u^2}} \tag{8}$$

and the stability condition leads to (see Appendix B):

$$(\Delta)(\Delta + \beta) > 0 \tag{9}$$

Several remarks can be made from these two conditions.

If the units have the same optimum, $\beta = 0$, the stability condition becomes $\Delta^2 > 0$, which is true for any Δ.

The stability is not affected by the value of γ. This in turn means that if a measurement error exists (deterministic or stochastic), the convergence is not affected.

Choosing a value of $|\Delta| > |\beta|$ will assure the stability of the multiunit scheme. However, if the value of Δ is smaller than this distance, then the sign of β and Δ should be the same.

If $\gamma = 0$, the multiunit closed-loop system will converge around the point $u^* = -\beta/\Delta$, which is the average of the optimum of the two units.

If $\beta = 0$, then $\boldsymbol{u}^* = -\frac{\gamma}{\Delta^2 \frac{\partial^2 J}{\partial u^2}}$. This indicates that, though the optima of the two units are identical, the solution will be off from the optimum. Moreover, for smaller Δ the solution will be further away.

Use of correctors in multiunit optimization with nonidentical units

As mentioned earlier, the multiunit scheme with nonidentical units can converge to equilibrium points that are quite far away from the real optimal values, especially when $\gamma \neq 0$. To avoid such an occurrence, a corrector could be used so as to push each unit to its respective optimum. In this work, it is assumed that $\beta \approx 0$.

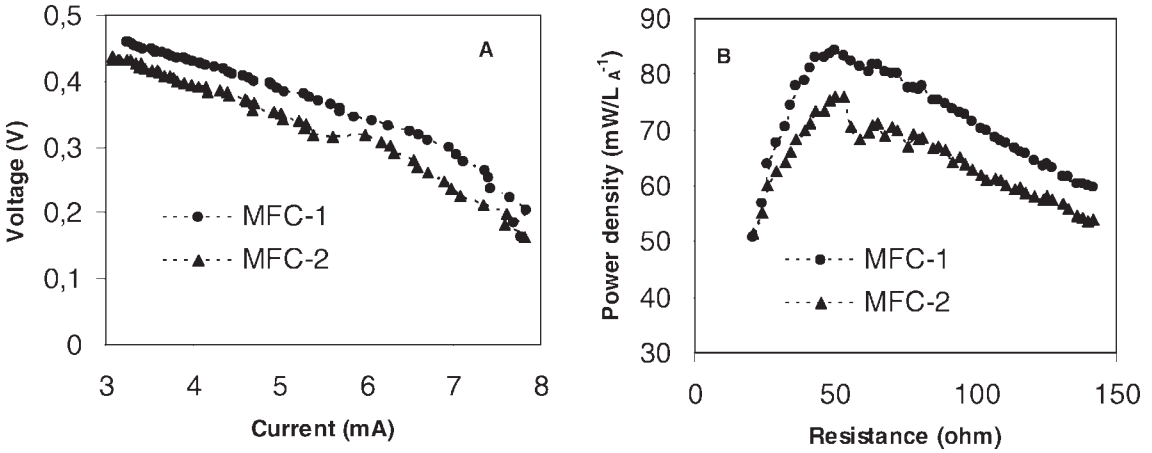

Figure 4. (A) Voltage as a function of current and (B) power density as a function of resistance.
The curves were obtained using 2.5 Ω step changes and a 10 min interval between resistance changes.

A correction of γ, $\hat{\gamma}$, is applied (Eq. 13). The idea is to bring the two units to the same input value from time to time and the difference between the outputs would represent the value of γ. For this, the idea is to alternate between the multiunit method and the calculation of the corrector. The fact that the scheme is in the multiunit mode or in the correction mode is indicated by a function d_{mu}.

$$d_{\text{mu}}(t) = \begin{cases} 1 & \text{if } i(T_1+T_2) \le t \le i(T_1+T_2)+T_1 \\ 0 & \text{if } i(T_1+T_2)+T_1 \le t \le (i+1)(T_1+T_2) \end{cases} \tag{10}$$

where $i \in Z$, T_1 is the time allotted for multiunit operation, and T_2 for correction. So, the two units are synchronized as follows:

$$\begin{aligned} u_1 &= u - \frac{\Delta}{2} d_{\text{mu}} \\ u_2 &= u + \frac{\Delta}{2} d_{\text{mu}} \end{aligned} \tag{11}$$

This means that there is a difference of Δ during the multiunit operation and no difference between them when calculating the correction for γ.

The multiunit adaptation law and the adaptation law for the corrector are given by

$$\dot{u} = k \frac{J_2 - J_1 - \gamma}{\Delta} d_{\text{mu}} \tag{12}$$

$$\dot{\hat{\gamma}} = k_\gamma (J_2 - J_1 - \hat{\gamma})(1 - d_{\text{mu}}) \tag{13}$$

where, k and k_γ are positive constants.

It has been shown in Ref. 26 that the equilibrium of the scheme described by Eqs. 12 and 13 on the average $(\boldsymbol{u}^e, \hat{\gamma}_e)$ is given by $\hat{\gamma}_e = \gamma$ and $u_e = u_1^{\text{opt}} = u_2^{\text{opt}}$, the real optimal points of operation. Also, these equilibrium points are locally asymptotically stable.

Results and Discussion

Polarization test

Before the test, both air–cathode MFCs were operated at an acetate load of 3.3 g/(L_A d) (A = anode volume), a temperature of 23°C, and an external resistance of 200 Ω. Under these conditions, stable performance was observed with a power density of 40–48 mW/L_A. Acetate concentration in the reactor effluent was measured at 300–400 mg/L, i.e., substrate nonlimiting conditions were provided. To compare performances of the two MFCs, polarization curves were acquired by applying step changes to digital resistors connected to each cell. First, the resistances were brought to 142 Ω and then decreased to 14 Ω in steps of 2.5 Ω. An interval of 10 min was allowed between the changes. Figure 4 shows the resulting polarization curves for MFC-1 and MFC-2. Linear parts of each polarization curve (Figure 4A) were used to calculate internal resistances, which were estimated at 45 Ω and 47 Ω for MFC-1 and MFC-2, respectively. Importantly, power output in a MFC is maximized when the external resistance is equal to the cell internal resistance,[9] therefore $\beta \approx 0$ in Eq. 7. However, at an optimal external resistance power densities were different (Figure 4B), therefore $\gamma \neq 0$. Finally, the curvatures around the optimum were similar, i.e., $\overline{\boldsymbol{J}}(\boldsymbol{u}) \approx 0$. Overall, the test demonstrated the importance of external load optimization in maximizing power output. Indeed, power output was decreased by 25% when increasing external load to 150 Ω from its optimal value of 45–47 Ω. Furthermore, MFC operation at external loads below its internal resistance resulted in abrupt power decrease (Figure 4B).

MFC dynamics

A comparison of the polarization curves obtained by decreasing external resistance from 142 to 14 Ω (sweep down) with the curve obtained by increasing the external resistance from 14 to 142 Ω (sweep up) showed similar results except that the sweep up curves were slightly below the sweep down curves (results not shown). This observation suggested that MFCs might not have reached steady state in the 10 min allowed between each resistance change. To understand the dynamics better, single step changes were applied at different operating points (Figure 5). These tests gave an estimation of the MFCs response time between 15 and 20 min. This response time is characteristic of microbial transformations and might reflect limitations of substrate transformation and electron transfer by anodophilic microorganisms.[2,5,7] Also, a fast component of the dynamics (within

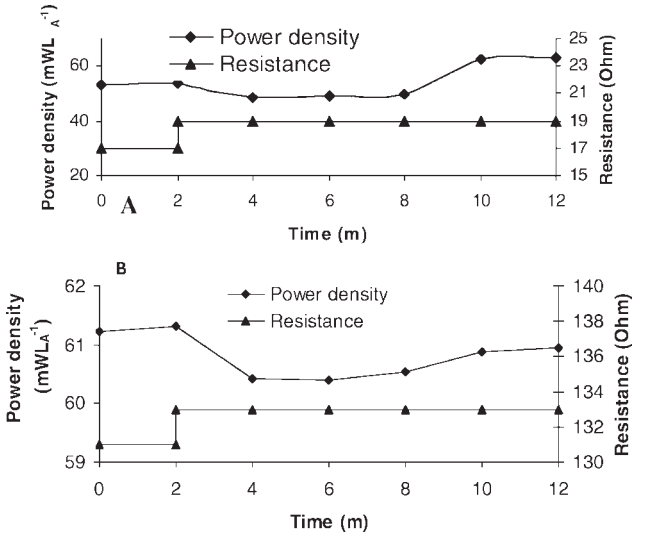

Figure 5. Power density variations in response to external resistance changes below the internal resistance value (A) and above the internal resistance value (B).

The curves were obtained in MFC-1 using step changes of 2.5 Ω with a 10 min interval between external resistance changes.

first several minutes after a step change) was observed. This component was associated with the electrochemical reaction.

An increase in external resistance immediately reduced output power and this immediate decrease was followed by a slow transition to a new steady state. The new steady-state output power could be either lower or higher than the value before the perturbation, depending on the region of operation. When the external resistance is below its optimal value, an increase in the resistance leads to a higher output power at steady state (Figure 5A). When the external resistance is above the optimal value, a further increase results in a decreased power at steady state (Figure 5B). Overall, the system behaves like an inverse response system when the external resistance is below its optimal value and without an inverse response for external resistances above the optimal value. This is typical of many nonlinear dynamic systems with an optimum.[27]

A comparison of bump tests similar to Figure 5 demonstrated that dynamics of the two MFCs are almost identical. This confirmed applicability of the multiunit optimization algorithm. A temporal perturbation method would require a waiting period of at least 10 to 15 min, i.e., the time needed for the inverse response effect to dissipate. With smaller time intervals, any decrease in resistance would instantaneously increase the power and push the resistance to its lower limit, thus missing the optimum. As the two MFCs featured similar dynamics. The finite difference algorithm used in the multiunit optimization method to estimate the gradient was expected to eliminate or minimize this dynamic effect. Consequently, the delay between the optimization steps can be significantly reduced.

Multiunit optimization

The multiunit optimization algorithm was applied to maximize power output according to the following objective function:

$$\max_{r} \boldsymbol{P} = \frac{\boldsymbol{U}^2}{\boldsymbol{r}} \tag{14}$$

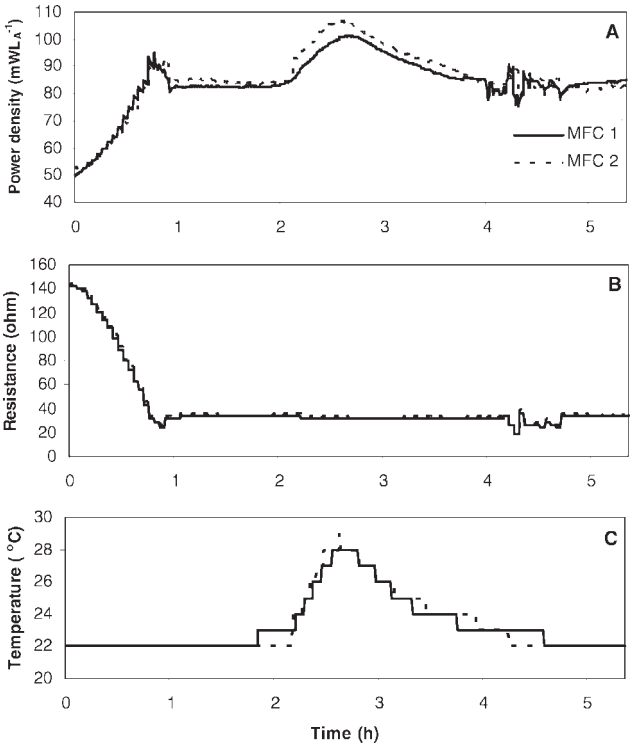

Figure 6. MFC behavior under a multiunit optimization algorithm.

where r is the value of the external resistance (Ω), P is the MFC power output (W), and U is the voltage measured at the terminals of the external resistor (V).

The multiunit optimization method with a γ corrector was applied. As $\beta \approx 0$, the choice of Δ for stability is not an issue here. Even a small value of Δ is suitable. For the optimization, a 3 min interval was used between each recalculation of the gradient and also between the recalculation of multiunit convergence and gamma corrector. The following tuning parameters, found by trial and error, were used in the test: $k = 90\ \Omega^2/\text{mW}$; $k_\gamma = 1$. Also, an average of four values acquired with 500 ms intervals was used for voltage measurements.

The optimization test was started at 140 Ω external resistances for both MFCs. Figure 6 shows the results of the multiunit optimization. In 1 h, the potentiometers were positioned around their optimal point of operation: 34 Ω for MFC 1 and 36 Ω for MFC 2 for a power output of 81.8 mW/L_A and 84.4 mW/L_A, respectively.

A comparison of internal resistances estimated using a polarization curve (Figure 4, 45 Ω for MFC 1 and 47 Ω for MFC 2) with the optimal resistance obtained by the multiunit algorithm (34 Ω for MFC 1 and 36 Ω for MFC 2, Figure 6) suggested the difference of about 10 Ω, which was attributed to the chosen method of γ estimation. It can be seen from Figure 4, that the difference between the two curves is not a constant and varies with the operating resistance. Therefore, the value of γ computed at one resistance value cannot be used for all resistance values.

Also, γ correction was performed with 3 min intervals. This means that the adaptation was done before steady state is reached. As r_1 is increased and r_2 decreased to reach the same value, the dynamics are opposing and when the difference is taken, they sum up rather than cancel each other. The accuracy of optimum estimation might be improved with increasing the interval used for γ corrections. In the

experimental results presented here, the value of the optimum was slightly underestimated. In another test, where an offset of opposite sign was used, the optimum was overestimated (+30 Ω), confirming the theory developed in Eq. 8 (results not shown).

Tracking the optimum under perturbations

Once the multiunit optimization algorithm had converged, a temperature perturbation was introduced into the process as shown in Figure 5 ($t = 1.9$ h). While the temperature was increased to 28°C the resulting optimal values were slightly reduced (by 2.5 Ω). After the temperature returned to 22°C, the potentiometers were set back to their previous optimal values by the optimization algorithm.

The interesting part of the multiunit scheme is the way it responds to temperature perturbation. Although the power increases drastically, and the temperature and its effect are in their transient phases, the scheme does not significantly change its operating point. This is due to the fact that it primarily relies on the difference between the outputs of the two units, which have similar dynamics. Consequently, the impact of the process dynamics on the algorithm convergence is minimized. However, the two MFCs were not identical and the return of temperature to its previous value was accompanied by dynamic differences. As a consequence, fluctuations around the optimal point were observed (Figure 6). Yet, the solution eventually converged to the optimal value.

Advantages of multiunit optimization

Electricity generation in a MFC is a microbiological process with relatively slow dynamics. The main advantage of the multiunit optimization algorithm was its fast convergence toward the optimum in comparison with other types of maximum power point tracking (MPPT) algorithms. For temporal perturbation algorithms, e.g., gradient-based or the perturbation-observation method,[14] each time step should be at least 10 min, so that the dynamics can pass beyond the inverse response phase. So, even assuming that the gradient values and the steps taken would be similar to that obtained by multiunit optimization, there is an immediate gain of a factor 3–4 compared with temporal perturbation methods. If we consider the perturbation-observation scheme in particular, which does not use the gradient information, just to get from the initial value of 140 Ω, to the optimal value of 40 Ω, with a step of 2.5 Ω every 10 min, it would take about 7 h, compared with 50 min obtained in this test.

The advantage of being insensitive to dynamics can also be reiterated in the case of temperature perturbations. As long as dynamics are identical, whether caused by external sources, or intrinsic dynamics, the optimization scheme does not get influenced by them. The heavy variations of the output that do not affect the optimal point are nicely filtered out by taking the difference.

Last but not least, the tuning and implementation of the multiunit controller is easy and straightforward. There are only two parameters to tune and they could be chosen fairly intuitively.

Conclusion

Low voltage and power density of a single MFC requires MFC stacking to produce significant amount of electricity. As in any other battery, MFC power output depends on the applied external load (resistance). As MFC is a biological system its internal resistance changes with time due to external perturbations, such as temperature, pH, and substrate composition. Consequently, maximization of MFC power output requires an on-line algorithm for tracking these variations. However, slow microbial transformations lead to relatively slow MFC dynamics and thus slow convergence of traditional optimization methods. Fast convergence of the multiunit optimization algorithm, which does not require steady state at each optimization step, is a clear advantage above the more traditional MPPT methods. A stack of nearly identical MFCs provides an ideal application for the multiunit optimization method.

This article presented the first application of the multiunit optimization algorithm to a stack of MFCs. Applicability of the method to a process with similar but nonidentical units has been successfully demonstrated. Future work should be extended toward developing a normalization procedure, which would allow for improved calculations of β and γ correctors.

Acknowledgments

This work is supported by the Natural Science and Engineering Research Council of Canada (NSERC) and National Research Council of Canada. (NRC publication no 49947). Assistance of Michelle Manuel in operating MFCs is greatly appreciated.

Literature Cited

1. Allen RM, Benetto HP. Microbial fuel-cells: electricity production from carbohydrates. *Appl Biochem Biotechnol*. 1993;39/40: 27–40.
2. Logan BE, Hamelers B, Rozendal RA, Schroder U, Keller J, Freguia S, Aelterman P, Verstraete W, Rabaey K. Microbial fuel cells: methodology and technology. *Environ Sci Technol*. 2006;40:5181–5192.
3. Reguera G, McCarthy KD, Mehta T, Nicoll JS, Tuominen MT, Lovley DR. Extracellular electron transfer via microbial nanowires. *Nature Biotechnol*. 2005;435:1098–1101.
4. Bond DR, Lovley DR. Electricity production by *Geobacter sulfurreducens* attached to electrodes. *Appl. Environ. Microbiol*. 2005;69:1548–1555.
5. Rabaey K, Boon N, Siciliano S, Verhaege M, Verstraete W. Biofuel cells select for microbial consortia that self-mediate electron transfer. *Appl Environ Microbiol*. 2004;70:5373–5382.
6. Logan BE, Regan JM. Electricity-producing bacterial communities in microbial fuel cells. *Trends Microbiol*. 2006;14:512–518.
7. Oh S-E, Logan BE. Voltage reversal during microbial fuel cell stack operation. *J Power Sources*. 2007;167:11–17.
8. Aelterman P, Rabaey K, Pham HT, Boon N, Verstraete W. Continuous electricity generation at high voltages and currents using stacked microbial fuel cells. *Environ. Sci. Technol*. 2006;40: 3388–3394.
9. Logan BE. *Microbial Fuel Cells*. Hoboken, NJ: Wiley; 2008: 200.
10. Marlin TE, Hrymak AN. Real-time operations optimization of continuous processes. *AIChE Symp Ser*. 1997;316:156.
11. Zhang Y, Monder D, Forbes JF. Real-time optimization under parametric uncertainty: a probability constrained approach. *J Process Control*. 2002;12:373–389.
12. Zhang Y, Forbes JF. Performance analysis of perturbation-based methods for real-time optimization. *Can J Chem Eng*. 2006;84: 209–218.
13. Sternby J. Adaptive control of extremum systems. *Can J Chem Eng*. 1980;24:151–160.

14. Blackman PF. An exposition of adaptive control, chapter extremum seeking regulators. In: Westcott JH, editor. *An Expasition of Adaptive Control Chapter: Extremum-seeking regulators*, New York: The Macmillan Company; 1962, pp. 36–50.
15. Krstic M, Wang H-H. Stability of extremum seeking feedback for general nonlinear dynamic systems. *Automatica*. 2000;36: 595–601.
16. Guay M, Zhang T. Adaptive extremum seeking control of nonlinear dynamic systems with parametric uncertainties. *Automatica*. 2003;39:1283–1293.
17. Hua C, Shen C. Comparative study of peak power tracking techniques for solar storage systems. *IEEE Appl Power Electron Conf Exposition Proc*. 1998;2:679–683.
18. Srinivasan B. Real-time optimization of dynamic systems using multiple units. *Int J Robust Nonlinear Control*. 2007;17:1183–1193.
19. Woodward L, Perrier M, Srinivasan B. Multi-unit optimization with gradient projection on active constraints. *Proc DYCOPS*. 2007;1:129–134.
20. Liu H, Logan BE. Electricity generation using an air-cathode single chamber microbial fuel cell in the presence and absence of a proton exchange membrane. *Environ Sci Technol*. 2004;38: 4040–4046.
21. Rozendal R, Hamelers HMV, Molenkamp RJ, Biusman CJN. Performance of single chamber biocatalyzed electrolysis with different types of ion exchange membranes. *Wat Res*. 2007;41: 1984–1994.
22. Tartakovsky B, Guiot SR. A comparison of air and hydrogen peroxide oxygenated microbial fuel cell reactors. *Biotechnol Prog*. 2006;22:241–246.
23. Nocedal J, Wright S. *Numerical Optimization*. New York: Springer; 1999.
24. Wang HH, Krstic M, Bastin G. Optimizing bioreactors by extremum seeking. *Int J Adapt Control Signal Process*. 1999; 13:651–669.
25. Guay M, Dochain D, Perrier M. Adaptive extremum seeking control of continuous stirred tank bioreactors with unknown growth kinetics. *Automatica* 2004;40:881–888.
26. Woodward L, Perrier M, Srinivasan B. Improved performance in the multi-unit optimization method with non units, *J Process Control*. DOI: 10.1016/j.jprocont.2008.04.010.
27. Van de Vusse JG. Plug flow reactor versus tank reactor. *Chem Eng Sci*. 1964;19:994–997.

Appendix A: Equilibrium Point With Two Nonidentical Units

The converged solution is given by $\hat{\boldsymbol{g}}(\boldsymbol{u}) = 0$, i.e., $\boldsymbol{J}_2(\boldsymbol{u}_2^*) - \boldsymbol{J}_1(\boldsymbol{u}_1^*) = 0$. So using Eqs. 5 and 7 gives

$$\boldsymbol{J}_1(\boldsymbol{u}_2^* + \beta) + \gamma + \overline{\boldsymbol{J}}(\boldsymbol{u}_2^*) - \boldsymbol{J}_1(\boldsymbol{u}_1^*) = 0 \qquad \text{(A1)}$$

Assuming $\overline{\boldsymbol{J}} = 0$, the second order Taylor series expansion around u_1^{opt} gives the following equation. Note that $\boldsymbol{u}_2^* = \boldsymbol{u}_1^* + \Delta$ and the zeroth and first order terms are zero or get canceled.

$$\frac{1}{2}\left(\frac{\partial^2 J_1}{\partial u^2}\right)(u_2^* + \beta - u_1^{\text{opt}})^2 + \gamma - \frac{1}{2}\left(\frac{\partial^2 J_1}{\partial u^2}\right)(u_1^* - u_1^{\text{opt}})^2 = 0 \qquad \text{(A2)}$$

$$\left(\frac{\partial^2 J_1}{\partial u^2}\right)(u_1^* - u_1^{\text{opt}})(\Delta + \beta) + \left(\frac{\partial^2 J_1}{\partial u^2}\right)(\Delta + \beta)^2 + \gamma = 0 \qquad \text{(A3)}$$

Then, the solution for $\boldsymbol{u}_1^*$ can be written as,

$$u_1^* = u_1^{\text{opt}} - \frac{\Delta + \beta}{2} - \frac{\gamma}{(\Delta + \beta)\frac{\partial^2 J_1}{\partial u^2}} \qquad \text{(A4)}$$

Since $\boldsymbol{u}^* = \boldsymbol{u}_1^* + \frac{\Delta}{2}$ and $u_1^{\text{opt}} - \frac{\beta}{2} = \frac{u_1^{\text{opt}} + u_2^{\text{opt}}}{2}$, $u^* \approx \frac{u_1^{\text{opt}} + u_2^{\text{opt}}}{2} - \frac{\gamma}{(\Delta+\beta)\frac{\partial^2 J_1}{\partial u^2}}$.

Appendix B: Stability Condition With Two Nonidentical Units

Applying the multiunit scheme described by Eqs. 5 and 6 to the system represented by Eq. 7 gives

$$\dot{\boldsymbol{u}} = \frac{\boldsymbol{k}}{\Delta}(\boldsymbol{J}_2(\boldsymbol{u}_2) - \boldsymbol{J}(\boldsymbol{u}_1)) \qquad \text{(B1)}$$

To evaluate the stability around the equilibrium $\boldsymbol{u}_1^*$ and $\boldsymbol{u}_2^*$, consider the Jacobian of the right hand side evaluated at the equilibrium. The Jacobian $\Im$ is given by:

$$\Im = \frac{\boldsymbol{k}}{\Delta}\left(\left.\frac{\partial \boldsymbol{J}_2}{\partial \boldsymbol{u}}\right|_{\boldsymbol{u}_2^*} - \left.\frac{\partial \boldsymbol{J}_1}{\partial \boldsymbol{u}}\right|_{\boldsymbol{u}_1^*}\right) \qquad \text{(B2)}$$

Using Eq. 7, considering a first-order Taylor series expansion of the derivative around u_1^{opt}, and neglecting $\frac{\partial^2 \overline{J}}{\partial u^2} \approx 0$, gives

$$\Im = \frac{\boldsymbol{k}}{\Delta}\left(\left.\frac{\partial \boldsymbol{J}_1}{\partial \boldsymbol{u}}\right|_{\boldsymbol{u}_2^*+\beta} + \left.\frac{\partial \overline{\boldsymbol{J}}}{\partial \boldsymbol{u}}\right|_{\boldsymbol{u}_2^*+\beta} - \left.\frac{\partial \boldsymbol{J}_1}{\partial \boldsymbol{u}}\right|_{\boldsymbol{u}_1^*}\right)$$

$$= \frac{\boldsymbol{k}}{\Delta}\left(\frac{\partial^2 \boldsymbol{J}_1}{\partial \boldsymbol{u}^2}(\boldsymbol{u}_2^* - \boldsymbol{u}_1^* + \beta) + \frac{\partial^2 \overline{\boldsymbol{J}}}{\partial \boldsymbol{u}^2}(\boldsymbol{u}_2^* - \boldsymbol{u}_2^{\text{opt}})\right)$$

$$\approx \frac{\boldsymbol{k}}{\Delta^2}\left(\frac{\partial^2 \boldsymbol{J}_1}{\partial \boldsymbol{u}^2}\right)\Delta(\Delta + \beta) \qquad \text{(B3)}$$

As $\boldsymbol{J}_1$ is a convex function, its second derivative is positive and so is the fraction $\frac{\boldsymbol{k}}{\Delta^2}$. So, the stability of the scheme is then guaranteed if $\Delta(\Delta + \beta) > 0$.

Manuscript received July 28, 2008, and revision received Aug. 4, 2008.